Journal of
Pharmacology & Clinical Toxicology

SciMedCentral

Special Issue on
Pharmacokinetics and Pharmacodynamics

Research Article

BNP7787 Forms Novel Covalent Adducts on Human Thioredoxin and Modulates Thioredoxin Activity

Aulma R Parker[1], Vicki L Nienaber[2], Pavankumar N Petluru[1], Vandana Sridhar[2], Betsy D Leverett[1], Philippe Y Ayala[1], Min Zhao[1], Barbara Chie-Leon[2], Kamwing Jair[1], Harry Kochat[1], John Badger[2] and Frederick H Hausheer[1]*

[1]*BioNumerik Pharmaceuticals, Inc., 8122 Datapoint Drive, Ste. 400, San Antonio, TX 78229*
[2]*Zenobia Therapeutics, Inc., 505 Coast Blvd South, Suite 111, La Jolla, CA 92037*

Abstract

We investigated the interactions between Thioredoxin (Trx) and BNP7787 (Tavocept®). BNP7787 is a water-soluble disulfide that appears well-tolerated and nontoxic, and in separate randomized multicenter Phase 2 and Phase 3 clinical trials in NSCLC patients, BNP7787 in combination with standard chemotherapy, resulted in substantial increases in the overall survival of patients with advanced adenocarcinoma sub-type NSCLC.

Activity assays indicate that BNP7787 and BNP7787-derived mesna disulfide heteroconjugates are novel alternative substrates of Trx with the potential to inhibit turnover of endogenous Trx substrates. LC-MS studies indicate that BNP7787 forms a covalent mixed-disulfide with Trx on cysteine residues 62, 69 and 73. BNP7787-modified Trx is less active than apo-Trx. X-ray crystallographic studies unequivocally confirm that BNP7787 forms stable mixed disulfides with Trx. BNP7787-modified Trx crystallized as a disulfide-linked tetramer with novel interactions between BNP7787-derived mesna and Trx, including stable BNP7787-derived mixed mesna-cysteine disulfides on human Trx resulting in unique, previously unidentified Trx structural conformations. Molecules A and B of the tetramer are identical to each other and exist in a conformation similar to other published Trx crystals. Molecules C and D, also identical to each other, undergo a significant conformational change relative to molecules A and B, and exhibit substantial disulfide reshuffling.

Inhibition or modulation of Trx by BNP7787 through covalent or non-covalent means may have important ramifications in cancers with elevated Trx activity, including adenocarcinoma sub-type NSCLC, and could impact Trx-related signaling pathways important for the inhibition of apoptosis and cell proliferation.

***Corresponding author**
Frederick H Hausheer, BioNumerik Pharmaceuticals, Inc., 8122 Datapoint Drive, Suite 1250, San Antonio, TX 78229, Tel: 210-614-1701; Fax: 210-614-0643; Email: fred.hausheer@bnpi.com

Submitted: 12 March 2014

Accepted: 23 March 2014

Published: 06 June 2014

Keywords
- Adenocarcinoma
- BNP7787 (Tavocept®; disodium-2, 2'-dithio-bis-ethanesulfonate, dimesna)
- Non-small cell lung cancer (NSCLC)
- Oxidoreductases
- Thioredoxin

Cite this article: *Parker AR, Nienaber VL, Petluru PN, Sridhar V, Leverett BD, et al. (2014) BNP7787 Forms Novel Covalent Adducts on Human Thioredoxin and Modulates Thioredoxin Activity. J Pharmacol Clin Toxicol 2(2):1026.*

ABBREVIATIONS

Cys: Cysteine; DTPA: Diethylene Triamine Pentaacetic Acid; DTT: Dithiothreitol; IPTG: Isopropyl β-D-1-Thiogalactopyranoside; LC-MS: Liquid Chromatography Mass Spectroscopy; NSCLC: Non-Small Cell Lung Cancer; PDB: Protein Data Bank; Prx: Peroxiredoxin; Trx: Thioredoxin; TrxR: Thioredoxin Reductase; TEV: Catalytic Domain of the Nuclear Inclusion a (NIa) Protein Encoded by the Tobacco Etch Virus.

INTRODUCTION

Thioredoxin (Trx) is the first member of the thioredoxin family of proteins. Trx possesses a fold which is comprised of a three layer α/β/α sandwich with a central four-stranded beta sheet surrounded by three alpha helices [1]. This structurally simple, yet functionally elegant fold exists in varying forms in many proteins and facilitates catalysis of a wide range of chemical reactions ranging from reductions of disulfides and peroxides to disulfide shuffling and mediation of glutathionylation/deglutathionylation events [1,2]. There are over 100 structure entries in the PDB for thioredoxin. The first Trx structure was elucidated by NMR in the early 1990's and contains five beta strands surrounded by four alpha helices [3]. The first crystal structure indicated that Trx assembled into a homodimers [4]. Trx, is a small disulfide containing protein that requires the selenoprotein, thioredoxin reductase (TrxR) for catalytic cycling [5]. Trx and TrxR along with thioredoxin peroxidase (peroxiredoxin, Prx) comprise the thioredoxin system [6]. Trx has important functions in the redox modulation of protein signaling and the reductive activation of transcription factors, including NF-κB, AP-1, and p53 [7-10]. Human Trx has 5 cysteine residues: Cys32 and Cys35 at the active site and Cys62, Cys69 and Cys73. Trx is active in its reduced form ($Trx-(SH)_2$) which serves as a hydrogen donor for ribonucleotide reductase and other redox enzymes [11]. A growing body of scientific data suggests that altered functioning of the thioredoxin system may contribute, directly or indirectly, to the development of cancer, tumor growth and angiogenic proliferation as well as resistance to chemotherapy-induced apoptosis [10, 12-14]. Modulation of Trx activity could have important ramifications for the development of more effective cancer therapies [13,14].

BNP7787 (Tavocept®, Disodium 2,2'-dithio-bis-ethanesulfonate; 1A) is a novel, water soluble disulfide that has been evaluated in clinical trials [15-25]. In separate randomized multicenter Phase 2 and Phase 3 clinical trials in NSCLC patients, treatment with BNP7787 in combination with standard chemotherapy, resulted in substantial increases in the overall survival of patients with advanced adenocarcinoma sub-type NSCLC in the first line treatment setting [26]. We hypothesize that BNP7787 and its metabolites may enhance antitumor activity of important chemotherapy agents in cancers that over express Trx and/or exhibit elevated Trx activity, by the direct inhibition, modulation, or inactivation of Trx. We have previously reported that thiol-containing drugs may dramatically disrupt the normal homeostatic thiol and disulfide balance both in the plasma and inside the cell and that they are often accompanied by toxic side effects [18]; however, for disulfide-containing drugs like BNP7787, there is no obvious mechanism through which they would substantially perturb the ratios of thiols and disulfides in these compartments. While BNP7787 is expected to remain predominantly in the disulfide form in the plasma, the intracellular environment and the interstitial space are likely venues for BNP7787 metabolism to mesna, mesna-disulfide heteroconjugates and free thiols [27,28] (Figure 1B).

Herein, we report that BNP7787 and BNP7787-derived mesna-disulfide heteroconjugates are novel alternative substrates of thioredoxin (Trx) with the potential to inhibit the turnover of endogenous Trx substrates, and that BNP7787-modified Trx is less catalytically active than apo-Trx. Additionally, LC-MS and X-ray crystallography data are presented showing that BNP7787-derived mesna covalently modifies Trx on Cys62, Cys69 and Cys73. To our knowledge, the Trx crystal structures described herein containing BNP7787-derived mesna-cysteine mixed disulfides are the first reported crystal structures showing a small molecule-derived mixed disulfide on human Trx. For crystal studies, we mutated 4 non-catalytic, non-structural residues in Trx (E13K, D16K, E95K and E103K) to facilitate crystallization of Trx at a pH where BNP7787-derived mesna adducts were stable (i.e., at pH 7.0 and higher; note that the crystals grown at higher pH values herein are essentially identical to crystals grown at pH 7.0). In the human Trx structures reported herein, we identify notable perturbations of the traditional thioredoxin fold and a shuffled disulfide bonding pattern when Trx is modified by BNP7787. Regulation of redox protein function by modification of cysteine residues includes cysteine directed glutathionylation, cysteinylation, homocysteinylation, nitrosylation, and many other modifications and is important in varied disease processes [29-31]. The posttranslational modification of cysteine residues in both redox and non-redox proteins, and the ensuing structural and functional consequences, is a widely studied area of research [32]. BNP7787-mediated mixed disulfide formation on select proteinaceous cysteine residues, resulting in altered molecular properties and/or function, may be a general mechanism of action for BNP7787.

MATERIALS AND METHODS

Materials

HPLC solvents were obtained from Burdick & Jackson (VWR). Glutathione and NADPH were purchased from CalBiochem (now Millipore) or SigmaAldrich. Trx and Rat thioredoxin reductase (TrxR) were obtained from SigmaAldrich (rat and human TrxR have > 90% sequence identity). Cysteinylglycine and γ-glutamylcysteine were purchased from Bachem. BNP7787 was prepared by a proprietary method (> 97%, no mesna was detected by mass spectroscopy). The heteroconjugates of mesna described herein were prepared by a solid-state synthesis method (≥ 98.3% pure) [33]. 10-20% Novex Tris-glycine gels, Tris-glycine native running buffer, Tris-glycine native sample buffer, native gel standards, and other gel electrophoresis items were purchased from Invitrogen. NAP5, NAP10 and PD Spin Traps were purchased from GE Healthcare. Trypsin Gold was purchased from Promega. Oligonucleotide primers used in cloning and mutagenesis were purchased from Valugene Roche Complete Protease Inhibitor tablets were purchased from Roche and benzonase was purchased from Novagen (EMD Biosciences) TEV protease was prepared at Zenobia. IPTG was purchase from Gold Biotechnology. Wild type and mutant thioredoxin proteins were purified from a pET-15b expression system. A Ni^{2+} charged IMAC

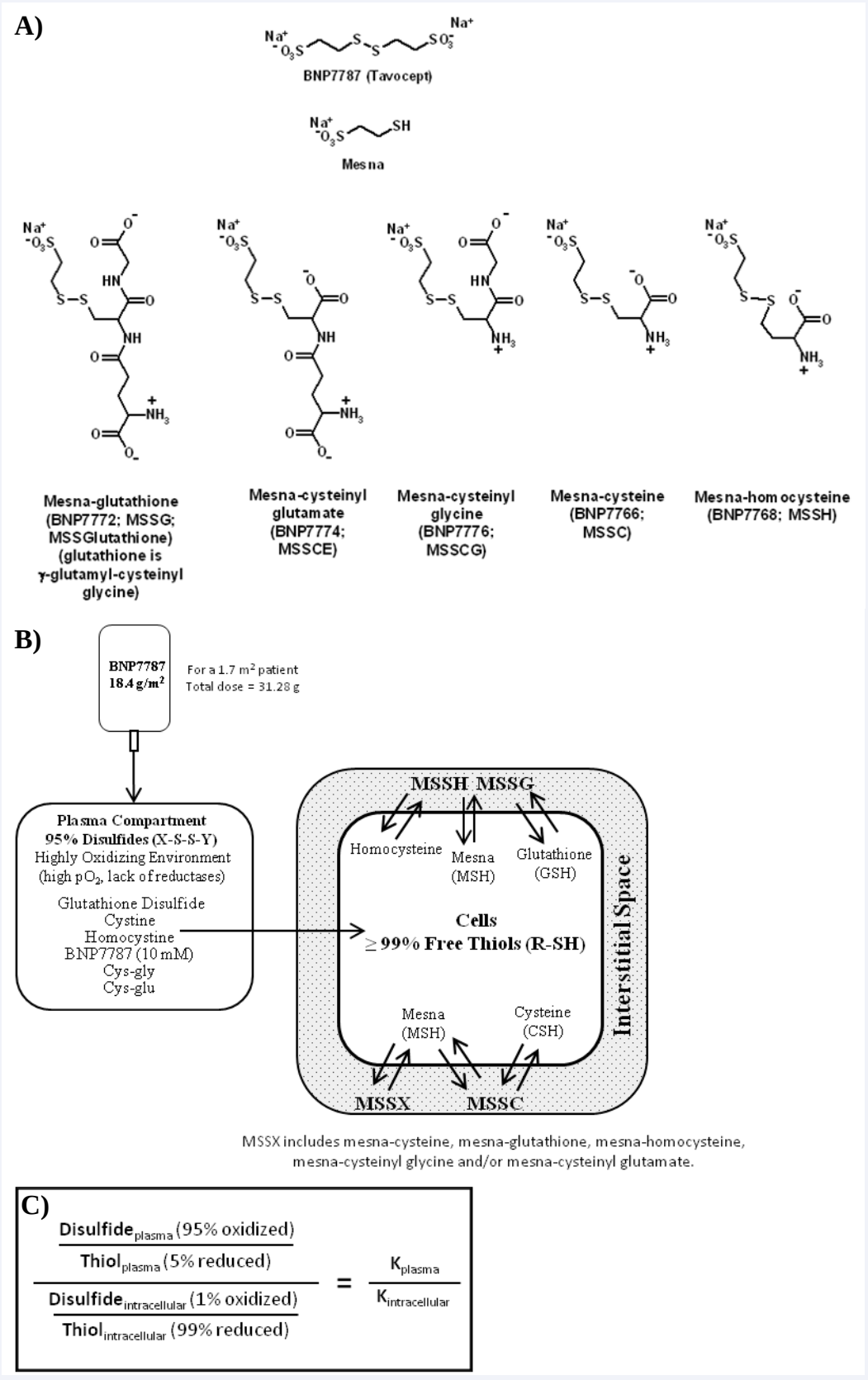

Figure 1 (A) Structures of BNP7787 (Tavocept®), mesna, and selected BNP7787-derived mesna-disulfide heteroconjugates. (B) BNP7787 thiol disulfide exchange reactions may occur intracellularly and/or in the interstitial space and (C) Relationship between thiol and disulfide balances in plasma and intracellularly.

resin was purchased from GE Life Sciences. PEGION, CRYSTALS HT, and PEGRX were purchased from Hampton Research, and JCSG and BASIC were purchased from JENA Biosciences. All other items were purchased from SigmaAldrich, ThermoFisher or MD Biosciences.

Evaluating the Effect of BNP7787 and BNP7787-derived mesna-disulfide heteroconjugates on Thioredoxin and Thioredoxin Reductase Activity Assays

The activities of TrxR and Trx were determined as described previously [34]. Assay mixtures contained TrxR Buffer (50 mM potassium phosphate, pH 7.0, 1 mM EDTA), 200 μM NADPH, 1.6 μg bovine TrxR, and one or more of the following: 4.8 μM human Trx, 86 μM insulin, and either the BNP7787 disulfide or one of the mesna-disulfide heteroconjugates (Figure 1A). Disulfides were added to reactions as 10x solutions in TrxR buffer. Reactions (volume 0.1 mL) were initiated by the addition of TrxR and were monitored at 25°C using a UV/vis plate reader. Activity was calculated using a 4 minute initial linear portion of each assay. Linear regression analyses, error calculations, and graphical representations were performed in Microsoft Excel.

Preparation of Thioredoxin with BNP7787-derived Adduct for MS Studies: Adduct Formation, Trypsin Digestion and Mass Spectroscopy Analyses

WT Trx (2.5 mg, 0.208 micromoles) was reduced using excess DTT (12.5 micromoles) in Tris buffer (100 mM, pH 8.0, 3 μL total volume) at 37°C for 50 minutes). DTT was removed using a G25 Sephadex column (GE Life Sciences) and the DTT-free, reduced protein was incubated with either BNP7787 (10 mM) or buffer alone at 37°C for 4 hours (reaction volumes were 500 μL or 1 mL). A G25 Sephadex column was used to remove unreacted small molecules. After gel filtration removal of the excess BNP7787, the Trx protein was digested in preparation for mass spectroscopy analyses. The G25 chromatographed Trx incubation reactions were digested with Trypsin Gold (9 μg/reaction, 12 hours, 37°C). Digested samples were analyzed using LC-MS, a Symmetry C18 HPLC column (Waters, Franklin, MA; 3.5 μm; 4.6 x 75 mm), and a Waters 2695 Alliance liquid chromatography system coupled to a Micromass single quadropole mass detector (Micromass ZMD, Manchester, UK) were used to analyze fragments from digested human Trx (mobile phase contained 0.1% of formic acid throughout the run; flow rate was 0.35 ml/min). The elution scheme was: Step 1: 0 to 3.5 minutes. mobile phase 95% water/5% acetonitrile; Step 2: 3.5 to 20 minutes linear gradient to 10%water/90%acetonitrile; Step 3: 20-30 minutes hold at 10% water/90% acetonitrile; and Step 4: 30-40 minutes linear gradient from 10% water/90% acetonitrile to 95% water;5% acetonitrile. Ionization modes across the mass ranges of 500 – 3000 Da (positive-ion mode) and 100 – 1700 Da (negative-ion mode) were used.

Preparation of BNP7787-modified Trx for Evaluation in Thioredoxin Activity Assays and Native Gel Electrophoresis

WT Trx (2.5 mg, 0.208 micromoles) was reduced using excess DTT (12.5 micromoles) in Tris buffer (100 mM, pH 8.0, 300 μL total volume) at 37°C for 50 minutes. DTT was removed using a Nap5 G25 Sephadex column (GE Life Sciences) and the DTT-free, reduced protein was aliquoted into incubations containing either BNP7787 (10 mM), glutathione disulfide (10 mM), or buffer alone at 37°C for 4 hours (reaction volumes were typically 150 μL). Prior to assaying, Trx incubated with buffer only (Trx-control), Trx incubated with BNP7787 (Trx-mesna), or Trx incubated with glutathione disulfide (Trx-GSH) were processed through PD Spin Traps to remove unreacted small molecules (BNP7787 or glutathione disulfide; note that buffer control was also processed to insure all samples received the same workup). The resulting samples, Trx-control, Trx-mesna, and Trx-GSH, were assayed using methods previously described [34]. For gel analyses, incubations were set up as described above, but at 0.5, 6, 24, and 48 hour incubation times, aliquots from each reaction (i.e., Trx incubated with buffer or Trx incubated with BNP7787) were removed and loaded onto gels.

Cloning and Site Directed Mutagenesis to produce the E13K, D16K, E95K, E103K Thioredoxin Protein

Wild-Type thioredoxin was cloned into a proprietary vector containing an N-terminal 6Xhis tag cleavable by TEV protease. Wild-type DNA underwent three rounds of mutagenesis using the following primers: E13K/D16K 5' GCA AAA CCG CTT TTC AGA AAG CTC TGA AGG CAG CCG GTG ACA AAC 3' and 5' GTT TGT CAC CGG CTG CCT TCA GAG CTT TCT GAA AAG CGG TTT TGC 3'; E95K 5' TCT CCG GCG CAA ACA AAA AAA AAC TGG AAG CAA CC 3' and 5' GGT TGC TTC CAG TTT TTT TTT GTT TGC GCC GGA GA 3'; E103K 5' AAA AAC TGG AAG CAA CCA TCA ATA AAC TGG TGT GAC TCG 3' and 5' CGA GTC ACA CCA GTT TAT TGA TGG TTG CTT CCA GTT TTT 3'. The final cloning product, Trx containing E13K, D16K, E95K and E103K mutations (r-Trx), was verified by DNA sequencing.

Protein Expression and Purification

The E13K, D16K, E95K and E103K Trx mutant was expressed in BL21 (DE3) cells. Cells were grown at 37°C to OD_{600} ~ 0.6. Protein expression was induced with 0.5 mM IPTG at 18°C overnight. Cell biomass was harvested and stored at -80°C until ready to use. Purification of target protein was done using a 3 column system. The cell biomass was lysed by sonication in Buffer A (50 mM Tris-HCl pH 7.8, 500 mM NaCl, 10% glycerol, 20 mM imidazole, 20 mM βME) containing 1 Roche Complete Protease Inhibitor Tablet, and Benzonase (20,000 units). Target protein was purified using a Ni^{2+} charged IMAC resin GE Lifesciences and eluted with imidazole (250 mM, pH 7.0). Peak fractions were cleaved with 2 mg TEV protease overnight in Buffer A. Cleaved protein was chromatographed over a Ni^{2+} charged IMAC resin collecting the flow-through. Aggregated oligomeric protein was separated from monomeric protein using size exclusion (S200 GE LifeSciences) in Tris buffer (50 mM, pH7.5) containing NaCl (250 mM) and DTT (5 mM). Monomeric protein was concentrated to ~60 mg/mL and additional DTT (50mM) was added. Protein was warmed to 30°C for 60 minutes to facilitate complete DTT-mediate reduction of disulfides. Protein not used immediately was flash frozen in liquid N_2 and stored at -80°C. The final purified protein contained an N-terminal sequence of GAGT which is part of the TEV recognition and cloning site. The last residue (threonine) of the tag was ordered in the electron density map. Activity assays evaluating the ability of the E13K, D16K, E95K,

E103K Trx protein (r-Trx) to reduce insulin were carried out as described previously [34].

Preparation and LC MS Analysis of BNP7787-derived mesna Adduct on Thioredoxin

Adduct was prepared based on the method described above with modifications designed to increase the likelihood of success in crystallization experiments. Briefly, r-Trx (E13K, D16K, E95K, E103K Trx; 60 mg/mL) in Tris (20 mM, pH 7.5), NaCl (250 mM) and DTT (5 mM) was fully reduced by adding a vast excess of DTT (final concentration 50 mM). This reaction was incubated for 1 hour at 30ºC followed by overnight incubation at 4ºC. Next, excess DTT was removed using ultrafiltration (Millipore 10kDa MWCO) to exchange the protein 5 times against glycine (50 mM, pH 9.0)/NaCl (250 mM). This exchanged solution was supplemented with DTPA (1 mM), Neocuprione (1 mM) and BNP7787 (40 mM) and then incubated at 4°C overnight at either pH 9.0 or pH 7.0. Aliquots of this solution were analyzed by ESI LC-MS to confirm the presence of adduct(s) prior to initiation of crystallization experiments. All LC-MS data were collected at the Scripps Center for Metabolomics (La Jolla, CA).

Crystallization of a BNP7787-derived Mesna Adduct on E13K, D16K, E95K, E103K Thioredoxin

BNP7787-derived mesna adduct(s) on r-Trx (E13K, D16K, E95K, E103K Trx) were prepared for crystallization at either pH 9.0 or pH 7.0. Crystals were grown at either pH 8.5 or 7.0 using the sitting drop vapor diffusion method in 96 well formats (Greiner plates) at 60 or 160 mg/mL thioredoxin with 1 mM DTPA, 1 mM neocuprione, 40 mM BNP7787 at 20°C. The initial broad screens produced crystals under a wide range of conditions (data not shown) and the screens used were PEGION, CRYSTALS HT, and PEGRX (Hampton Research) and JCSG, and BASIC (JENA Biosciences). Multiple rounds of optimization were completed and included fine screens, varying the protein concentration and varying the protein to reservoir ratios to obtain diffraction quality crystals. In r-Trx pH 9.0/8.5 structure (adduct formed at pH 9.0, crystals grown at pH 8.5), the best crystals were obtained in 20% ethanol, 0.1 M Tris (at 60 mg/mL r-Trx protein) and diffracted to 2.5 Å (C2 space group). In r-Trx pH 9.0/7.0 (adduct formed at pH 9.0, crystals grown at pH 7.0), the best crystals were obtained in 20% PEG3350, 0.2 M KCl (60 mg/mL Trx protein) and diffracted to 2.8 Å (C2 space group). In r-Trx pH 7.0/7.0 (adduct formed at pH 7.0, crystals grown at pH 7.0), the best crystals were obtained in 28% PEG3350, 0.2 M KCl (160 mg/mL r-Trx protein) and diffracted to 1.85 Å resolution ($P2_1$ space group).

Structure Solution and Refinement

Diffraction data were collected at a wavelength of 1.0Å on a Rayonix 225 detector array at beamline LS-CAT 21ID-F at the Advanced Photon Source (Argonne National Laboratory) or on an ADSC Q315R detector at beamline 5.0.1 at the Advanced Light Source (Lawrence Berkeley National Laboratory). Data were indexed, integrated, scaled and merged using the programs HKL2000 or Mosflm (Table 2). The pH 9.0/8.5 structure was solved by molecular replacement with PHASER using a monomer from the Protein Data Bank (PDB) entry for human Trx (PDB ID: 2HXK) as the search model. The solution was consistent with four molecules in the crystal asymmetric unit. The protein model was iteratively refit and refined using MIFit (MIFit Open Source Project, 2010, http://code.google.com/p/mifit) and REFMAC5 [35]. Molecules C and D were substantially rebuilt and the BNP7787-derived mesna adduct added after protein rebuilding was complete. The structure solution is supported by contiguous electron density for the entire chain trace of each molecule, landmark side chain density features matching the amino acid sequence including cysteines, absence of phi-psi violations and final R/Rfree values in the normal range. The structure showed an unusual conformation and disulfide formation for two of the four protein molecules in the crystal asymmetric unit. For the r-Trx pH 9.0/8.5 structure, residual density observed near Cys69 of molecule A was modeled as a BNP7787-derived mesna adduct in a dual conformation. The two additional structures (r-Trx pH 9.0/7.0 and r-Trx pH 7.0/7.0) were solved by molecular replacement (PHASER) using portions of the r-Trx pH 9.0/8.5 structure as a search model. For the r-Trx pH 9.0/7.0 structure, residue density observed near Cys69 of molecules A and B and Cys62 of molecules A and B was modeled as BNP7787-derived mesna adducts (two orientations for Cys69 adduct; single orientation for Cys62 adduct). For the r-Trx pH 7.0/7.0 structure, residual density observed near Cys69 of molecules A and B was modeled as a BNP7787-mesna adduct. For the r-Trx pH 9.0/8.5 and r-Trx pH 9.0/7.0 structures, residual density at the N-terminus was modeled as a Thr residual from the TEV recognition site. An additional Gly-Thr was observed in the highest resolution structure (r-Trx pH 7.0/7.0). Final statistics for the refined structures are summarized in Table 3.

Accession Numbers

PDB codes are **4POK** (Trx structure with adduct formation at pH 9.0 and crystallization at pH 8.5; 2.5 Å), **4POL** (Trx structure with adduct formation at pH 9.0 and crystallization at pH 7.0; 2.8 Å), and **4POM** (Trx structure with adduct formation at pH 7.0 and crystallization at pH 7.0; 1.85 Å).

RESULTS

BNP7787 and BNP7787-derived mesna-disulfide heteroconjugates are alternative substrates of thioredoxin (Trx)

Although Trx exhibits a preference for insulin and other proteins as substrates [6,9,36-38], we hypothesized that Trx might catalyze the reduction of the disulfide bond in BNP7787 and/or in BNP7787-derived mesna-disulfide heteroconjugates. BNP7787 and BNP7787-derived mesna disulfide-heteroconjugates (Figure 1) were readily reduced by Trx in the presence of Thioredoxin reductase (TrxR) and NADPH (Table 1, Reaction B). In contrast, TrxR alone did not detectably reduce BNP7787 or BNP7787-derived mesna-disulfide heteroconjugates (Table 1, Reaction A). BNP7787 and BNP7787-derived mesna-disulfide heteroconjugates (Figure 1A) probably lack structural functionalities needed to serve as effective substrates for TrxR directly, despite the fact that TrxR can accept a broad range of substrates [8,38].

The BNP7787-derived mesna-disulfide heteroconjugates mesna-glutathione (MSSG), mesna-cysteine (MSSC) and mesna-

Table 1: BNP7787 and BNP7787-derived Mesna-Disulfide Heteroconjugates in Thioredoxin (Trx) and Thioredoxin Reductase (TrxR) Activity Assays.

Reaction A $X-SS-Y + NADPH + H^+ \xrightarrow{TrxR} NADP^+ + XSH + YSH$

Reaction B $X-SS-Y + NADPH + H^+ \xrightarrow{TrxR + Trx} NADP^+ + XSH + YSH$

Disulfide (0.5 mM)	NADPH Oxidation (nmoles/min/mL)[a,b]	
	Reaction A[c]	Reaction B
No Disulfide (background control)	0.14 ± 0.01	0.30 ± 0.04
BNP7787	0.3 ± 0.01	13.1 ± 0.2
(MSSG) MSSGlutathione	0.3 ± 0.02	14.1 ± 0.1
MSSC	0.2 ± 0.03	14.4 ± 0.2
MSSH	0.0 ± 0.03	8.6 ± 0.06
[d]MSSCE	0.3 ± 0.02	9.6 ± 0.2
[d]MSSCG	0.2 ± 0.04	15.8 ± 0.3

[a] Oxidation rates were calculated from the 4 minute change in absorbance and triplicate or more assays.
[b]A two-way ANOVA analysis was performed on the whole dataset. The difference between reaction rates for type A reactions and type B reactions is statistically significant (p-value = .0001), and affected by the disulfide substrate used in the reaction (p-value = .0001).
[c]Zero is assigned to rates calculated from positive absorbance changes or from absorbance changes of less than .0001.
[d]The MSSCE and MSSCG compounds are mesna adducts of the cysteinyl-glutamate and cysteinyl-glycine intermediates in the biosynthesis and degradation of GSH, respectively.
Refer to Figure 1 for structures of each disulfide.

cysteinylglycine (MSSCG) were preferred slightly by Trx over mesna-homocysteine (MSSH) and mesna-cysteinylglutamate (MSSCE), although all of the BNP7787-derived mesna-disulfide heteroconjugates were reasonably good Trx substrates (compare NADPH oxidation values for reaction A in Table 1 (i.e., TrxR alone) to NADPH oxidation values for reaction B in Table 1 (TrxR in combination with Trx)). As alternative substrates of Trx, BNP7787 and BNP7787-derived mesna-disulfide heteroconjugates may potentially inhibit turnover of endogenous Trx substrates.

LC-MS indicates that BNP7787 forms covalent mesna-adducts with cysteine residues in thioredoxin (Trx)

Several groups have reported that modification of cysteine residues in Trx result in inactivation of Trx or impair Trx activity or functioning [39-41]. Casagrande et al. have previously reported a glutathione-Trx adduct on cysteine-73 (Cys73) of Trx that they proposed may be involved in mediating crosstalk between the Trx and Grx systems [39]. Trx was incubated with either buffer only (control), BNP7787, or glutathione, and, prior to tryptic digests, excess/unreacted BNP7787 and glutathione were removed in a size exclusion step. After digest with trypsin, Trx fragments were analyzed by liquid chromatography mass spectrometry (LC-MS) for BNP7787-derived mesna-cysteine adducts (Figure 2 A-C). In control reactions with glutathione, as previously reported by Casagrande et al. [39], Trx was glutathionylated at Cys73 (data not shown). LC analysis revealed a new peak in the reactions incubated with BNP7787 or mesna (Figure 2 D-E); MS analyses of these new peaks revealed the presence of a mesna adduct on Cys73 of Trx (CMPTFQFFK Trx fragment, Figure 2D). An additional mesna adduct on the Trx tryptic fragment containing Cys62 and Cys69 was detected (fragment YSNVIFLEVDVDDCQDVASECEVK, Figure 2E); however, attempts to identify which cysteine in this 24 residue-fragment contained the mesna adduct (i.e., Cys62 or Cys69) were unsuccessful and served as the impetus for pursuing the X-ray crystallographic studies described herein.

BNP7787 mediated modification of Trx results in a decreased rate for the Trx/TrxR coupled assay and altered Native gel electrophoresis profile

When BNP7787 is present in the Trx/TrxR assay, strong turnover of NADPH occurs as BNP7787 is reduced to mesna (Table 1). This NADPH turnover in the presence of BNP7787 does not require insulin, indicating that BNP7787 is an alternative substrate for the Trx/TrxR system and can act as a competitive inhibitor relative to other substrates. To evaluate the effect of the covalent modification of Trx by BNP7787 on protein activity, unreacted BNP7787 must be removed (see Methods section). Gel filtration purified Trx-mesna was assayed using methods described previously [34]. Apo-Trx (Trx-control), BNP7787-treated (Trx-mesna), and Glutathione disulfide-treated (Trx-GSH) samples (see Methods section for preparation) were analyzed (triplicate reactions) in the Trx/TrxR coupled assay following NADPH-dependent reduction of the insulin AB disulfide. NADPH oxidation rates for varying concentrations of Trx incubated with either buffer (apo-Trx aka Trx-control), BNP7787 (Trx-mesna), or glutathione disulfide (Trx-GSH) were converted to a percentage scale, where the Trx-control for each Trx concentration tested was assigned a 100% value (Figure 3A). Both Trx-Mesna and Trx-GSH are inhibited, relative to a Trx-control, indicating that the mesna or GSH adduct on Trx is interfering with the reduction of insulin AB disulfide. Additionally, Trx samples incubated with buffer migrated as a high molecular weight smear on non-denaturing, non-reducing Native gels (Figure 3B, lanes 2, 4, 6, and 8) most likely due to various disulfide bonding interactions of apo-Trx that can occur under these gel conditions. Trx incubated with BNP7787 (Figure 3B, lanes 3, 5, 7, and 9) had distinct bands corresponding to a tetramer (labeled A) and dimer (labeled B). At longer incubation times, a third band appeared (labeled C) and likely corresponds to a monomer. Native gels are run in the absence of detergent and reductant; however, in one experiment we added DTT to all Trx samples immediately prior to loading on Native gels and this resulted in an identical migration profile for

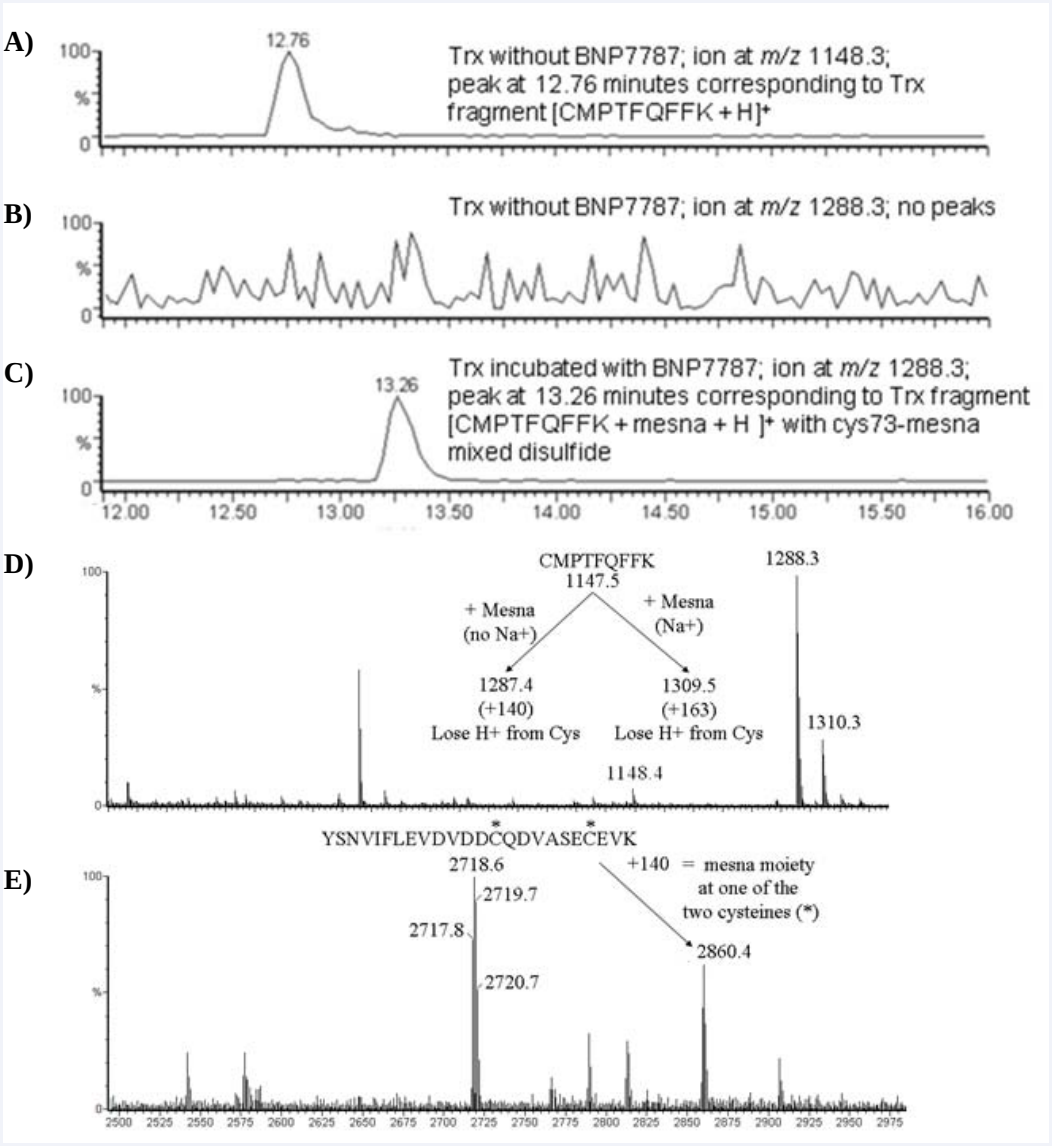

Figure 2 LC/MS Analysis of Tryptic fragments with Trx cysteines containing BNP7787-derived mesna moieties. (A) Trx incubated without BNP7787 ion at *m/z* 1148.3; retention time of 12.76 minutes corresponding to fragment [CMPTFQFFK + H]$^+$; (B) Trx incubated without BNP7787 or mesna does not have ion at *m/z* 1288.3 and no peaks corresponding to [CMPTFQFFK + Mesna + H]$^+$); (C) Trx incubated with BNP7787; ion at *m/z* 1288.3 with retention time of 13.26 minutes corresponding to fragment [CMPTFQFFK + Mesna + H]$^+$ with cysteine-73-mesna adduct; (D) the positive-ion MS for Trx fragments containing covalent mesna adducts from reactions where Trx was incubated with BNP 7787 for cysteine-73-mesna adduct at ions of *m/z* 1288.3 [CMPTFQFFK + Mesna + H]$^+$ and *m/z* 1310.2 [CMPTFQFFK + Mesna + Na + H]$^+$, respectively; (E) the positive-ion MS for Trx fragments containing covalent mesna adducts from reactions where Trx was incubated with BNP 7787 for identification of a mesna adduct in trypsin digested Trx fragment containing cysteine-62 and cysteine-69 at ions of *m/z* 2718.6 [YSNVIFLEVDVDDCQDVASECEVK + H]$^+$ and *m/z* 2860.4 [YSNVIFLEVDVDDCQDVASECEVK + Mesna + H]$^+$, respectively.

all Trx samples (i.e., Trx incubated with and without BNP7787) as would be expected. Under denaturing, reducing SDS PAGE conditions, all samples migrate as a monomer (Figure 3D).

Engineering E13K, D16K, E95K, E103K thioredoxin for crystallization

Wild-type human thioredoxin contains 17 aspartic and glutamic acid residues, 12 lysine residues, and has a predicted pI of 4.82 (predicted using Compute pI). In preliminary experiments, quality Trx crystals did not grow at pH 7.0 or higher; however, the BNP7787-derived mesna adduct on Trx was more stable at pH values of 7.0 or higher (data not shown). To facilitate crystal growth at pH values closer to 7.0, we engineered mutant Trx proteins, with elevated pI values. Examination of the surface of the Trx dimer (**PDB ID: 1ERT**) revealed three notable negatively charged patches (Figure 4). The largest negatively charged patch was located at or around the cluster of thiol groups near alpha helix 3 (Figure 4). Because BNP7787 was expected to react with one or more cysteine residues and because Cys32 and Cys35 are known to play an important role in catalysis, this region was not considered for mutagenesis. However, two additional

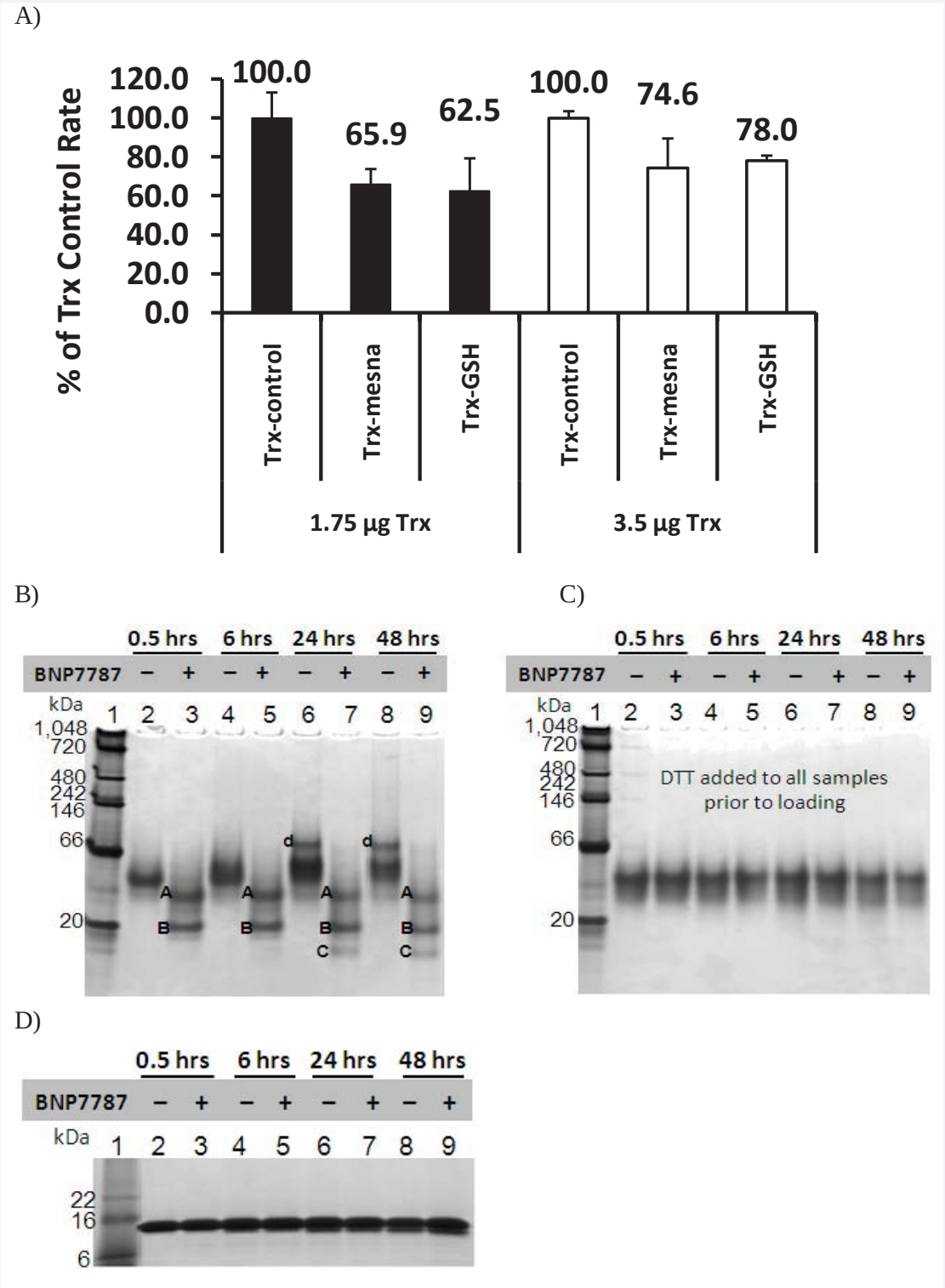

Figure 3 Trx protein modified by BNP7787 is inhibited relative to non-modified control and migrates distinctly in Native gels relative to unmodified Trx. (A) NADPH oxidation rates for varying concentrations of Trx incubated with either buffer (Trx-control), BNP7787 (Trx-mesna), or glutathione disulfide (Trx-GSH) . Rates were converted to a percentage scale; the Trx-control for each Trx concentration tested was assigned a 100% value and Trx-mesna and Trx-GSH assays are compared to this control. (B) Native gel analysis of Trx incubated with either buffer (-) or BNP7787 (+) for the times indicated. Bands corresponding to tetramer (band labeled A) and dimer (band labeled B) are visible in BNP7787 containing samples. Band C likely corresponds to a monomer and band d is likely a higher order oligomer. (C) PAGE Analysis of Trx incubated with either buffer (-) or BNP7787 (+) using Native gels where DTT, which fully reduces all disulfides, was added to all samples prior to electrophoresis. Note that under these conditions all samples have similar mobility that is essentially identical to Trx control in lane 1 of panel B. (D) Under denaturing, reducing SDS PAGE conditions, all samples migrate as a monomer.

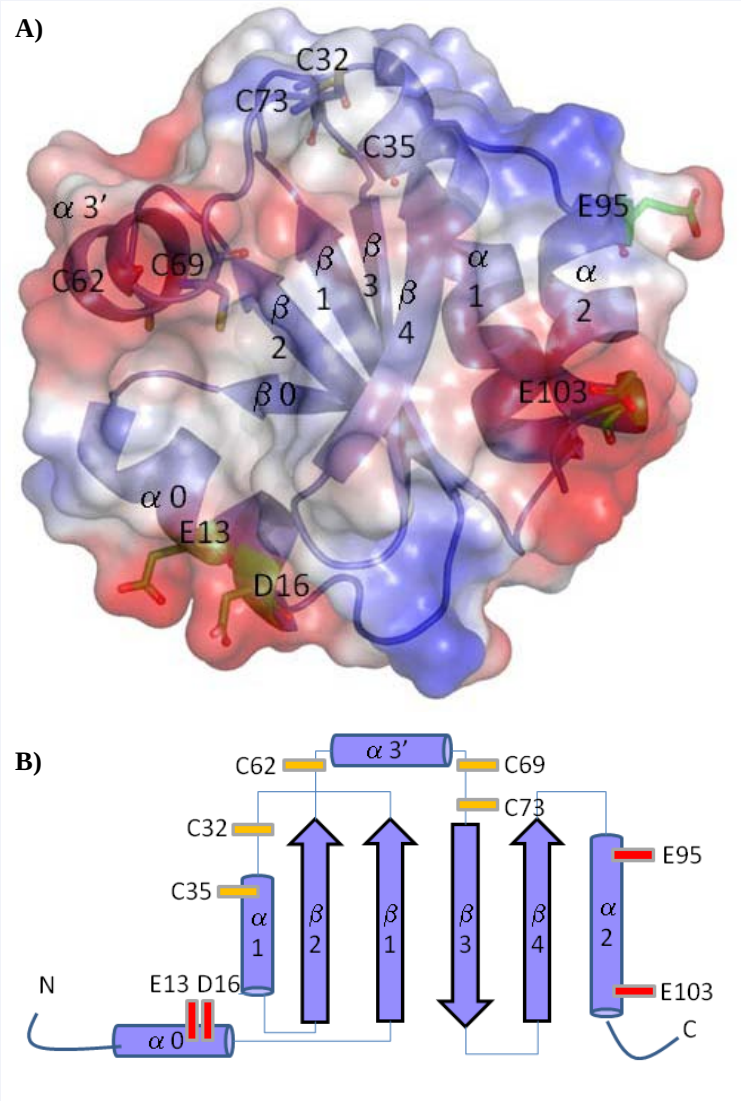

Figure 4 (A) Crystal structure of Trx-1 (PDB 1ERT) with an electrostatic surface showing three patches of negative charges. The four residues mutated to raise the pKa of the protein are shown as green sticks. Cysteine residues are shown as blue sticks. (B) Overall topology of the standard Trx fold showing the sites of cysteine residues and of our mutations.

negative patches were located opposite to the active site on surface exposed helices α0 and α2 (Figure 4). In both cases, two negatively charged residues were not involved in any salt bridges or hydrogen bonds, thus making them good candidates for mutagenesis. The first of these negative patches, included D16 and E13 (α0) and the second included E95 and E103 (α2). To adequately raise the pI of the protein, all four residues were mutated to lysines and the resulting quadruple (E13K, D16K, E95K, E103K) Trx mutant (abbreviated r-Trx herein) was predicted to have a pI of 8.59 making it a strong candidate for crystallization at pH values of 7.0 and higher. Activity assays evaluating the ability of the r-Trx protein to reduce insulin were carried out as described previously [34]. Activity of the r-Trx was found to be comparable to WT Trx activity (19.3 ± 1.45 and 22.4 ± 3.6 nmoles/min/mL, respectively, for 5.2 μg protein, 0.1 mL volume assay); therefore, the mutated residues did not impact r-Trx function.

Crystal structure of human Trx crystallized in the presence of BNP7787 at neutral or high pH

X-ray crystallographic analyses elucidated the three-dimensional structure of human r-Trx to identify the site of BNP7787 adduct formation at the following combinations: pH 9.0/8.5, pH 9.0/7.0, or pH 7.0/7.0. The r-Trx pH 9.0/8.5 structure diffracted to 2.5 Å (C2 space group). The r-Trx pH 9.0/7.0 structure diffracted to 2.8 Å (C2 space group). The r-Trx pH 7.0/7.0 structure, diffracted to 1.85 Å resolution ($P2_1$ space group). We were able to identify two sites of BNP7787 adduct formation (Cys62 and Cys69). However, in the course of these experiments, we also identified a previously unreported tetrameric structure for the r-Trx under all three conditions for adduct formation (Figure 5). All three r-Trx structures are highly similar (RMSD of 0.533 for r-Trx pH 9.0/8.5 and r-Trx 7.0/7.0 and

RMSD of 1.08 Å for r-Trx pH 9.0/7.0 and Trx 7.0/7.0). The overall structure of the tetramer will be described below with details of the adduct formation at the three pH combinations.

Description of the tetramer

In all three structures, the molecules composing the tetramer are covalently linked via intermolecular disulfide bonds. Two of the r-Trx molecules, A and B, in each r-Trx have the standard Trx fold (Figure 4, reviewed in reference 42). Molecules C and D of each r-Trx tetramer are in a conformation previously unreported for r-Trx, but identical and symmetric to each other. Below we discuss the main features of Trx molecules C and D and compare with the standard Trx fold which we observe for molecules A and B. We also describe the interfaces between the r-Trx molecules within the tetramer.

Conformational differences in molecules A and B versus molecules C and D

An overlay of molecule A (dark blue) and molecule C (pink) illustrating the structural differences between molecules A/B and C/D is shown in Figure 5B. The most significant changes are at helices α3 and α1 which unwind to form the tetramer interface. In molecules C/D, the α3 helix containing Cys62 and Cys69 (residues 62-69) of the standard Trx fold (Figure 4) unwinds to form an extended loop followed by a new beta strand (β2A, residues 68-72). The extended loop of molecules C/D binds near the active site of molecules A/B forming an intermolecular disulfide between Cys62 from molecules C/D to Cys73 from molecules A/B (Figure 5). In molecules C or D, Cys73, located at the end of the new beta strand (β2A), forms an intramolecular disulfide bridge with Cys35 in molecules D or C respectively (see

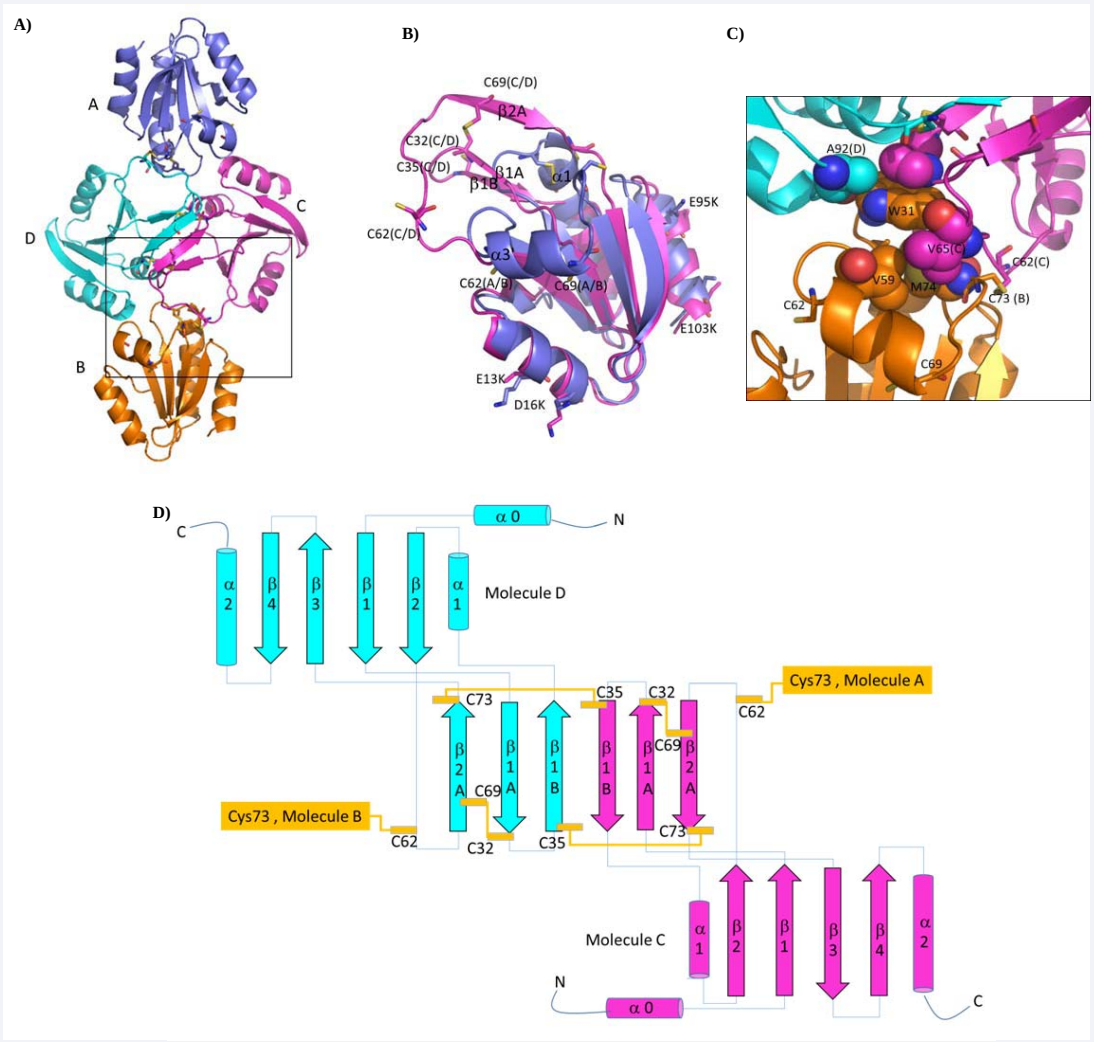

Figure 5 (A) Ribbon diagram representing the r-Trx-1 tetramer observed in our studies. The diagram is labeled and color coded to depict the molecules of the tetramer. (B) Overlay of molecule A and molecule C of the tetramer showing a significant local conformational change at helices α3' and α1. (C) Close-up of the hydrophobic core of the interface of molecules B and C depicting how the newly formed loop of molecule C interacts with molecule B. (D) Topology diagram depicting the modified fold observed for molecules C (pink) and D (cyan). Disulfide bridges are represented by yellow boxes and lines. New secondary structure elements were named according to their location within the r-Trx monomer. The new beta-barrel motif of the interface between C and D represented in the center of the diagram.

Figure 5D for schematic diagram of the new fold and disulfide bridges). There are also a series of hydrophobic interactions between Val65 of molecules C/D with Trp31, Val59 and Met74 of molecules A/B (Figure 5C) to form the core of the interface between the two domains. Strand β2A contributes to a new intramolecular structural domain consisting of a disulfide rich six stranded beta barrel with three strands from molecule C and three from molecule D (Figure 5D, Figure 6 discussed further below).

The second site of significant conformational change in molecules C/D occurs at the active site loop containing Cys32 and Cys35 and α1. The loop and part of α1 rearrange to form a two stranded beta sheet [β1A (29-32) and β1B (35-38)] with Cys35 (β1B) and Cys73 (β2A) making intramolecular disulfides between molecules C and D as discussed above (Figure 5D). Cys32 of β1A makes an intramolecular disulfide bond with Cys69 (β2A). Strands β1A and β1B also contribute to the newly formed six stranded beta barrel (Figure 5D, Figure 6).

Beta-barrel at the interface of C and D

A close-up of the beta barrel at the interface of molecules C and D is shown in Figure 6. Residues not contributing to the structural motif have been removed from the figure for clarity. The six stranded β-barrel is composed of three strands from each monomer (Figure 5, Figure 6). The barrel motif is stabilized by four disulfide bonds (Figure 5D, Figure 6A): two intramolecular, Cys69(C) – Cys32(C) and Cys69(D) – Cys32(D); and two intermolecular, Cys 35(C) – Cys73(D) and Cys35(D) – Cys73(C). The intermolecular disulfides form the top and bottom of the barrel. The barrel is further stabilized by a series of hydrophobic residues located in the core of the motif (Figure 6B). These residues include Met37 from molecules C and D (found in two distinct conformations), Thr30 (C and D) and Val71 (C and D) (see Figure 6B).

Formation of the beta barrel results in a number of new disulfide bonds when compared with the classical Trx fold. In the previously reported fold, all of the cysteine residues are not involved in disulfide bridges apart from the active site cysteines (Cys32, Cys35) which cycle between an oxidized and reduced form (see Figure 4). However, all of the cysteine residues in molecules C and D are involved in non-standard (for Trx) disulfide bonds (Figure 5D). In molecules A and B, Cys73 makes a new disulfide bridge with Cys62 of molecule C or D, respectively. The residues that were mutated to increase the pI and facilitate crystallization under neutral pH and higher pH conditions (i.e., E13K, D16K, E95K and E103K) are remote from the structural changes relative to the previously reported X-ray structures.

BNP7787-derived mesna binding site

For all three structures reported, all of the cysteine residues for molecules A, B, C and D are involved in protein disulfide bridges except for Cys62 and Cys69 in molecules A and B (which have the standard Trx fold). r-Trx was incubated with BNP7787 in advance of the co-crystallization experiments so, in principle, all of the cysteine residues were exposed to BNP7787. In all three r-Trx structures, a BNP7787-derived mesna adduct was observed on Cys69 for molecules A and B. In the r-Trx pH 9.0/7.0 structure, the adduct at Cys69 was modeled in two orientations. The r-Trx pH 9.0/7.0 structure contains a second BNP7787-derived mesna adduct on Cys62 for molecules A and B. There was no evidence of a mesna adduct on Cys62 for the other two structures at pH 9.0/8.5 and pH 7.0/7.0.

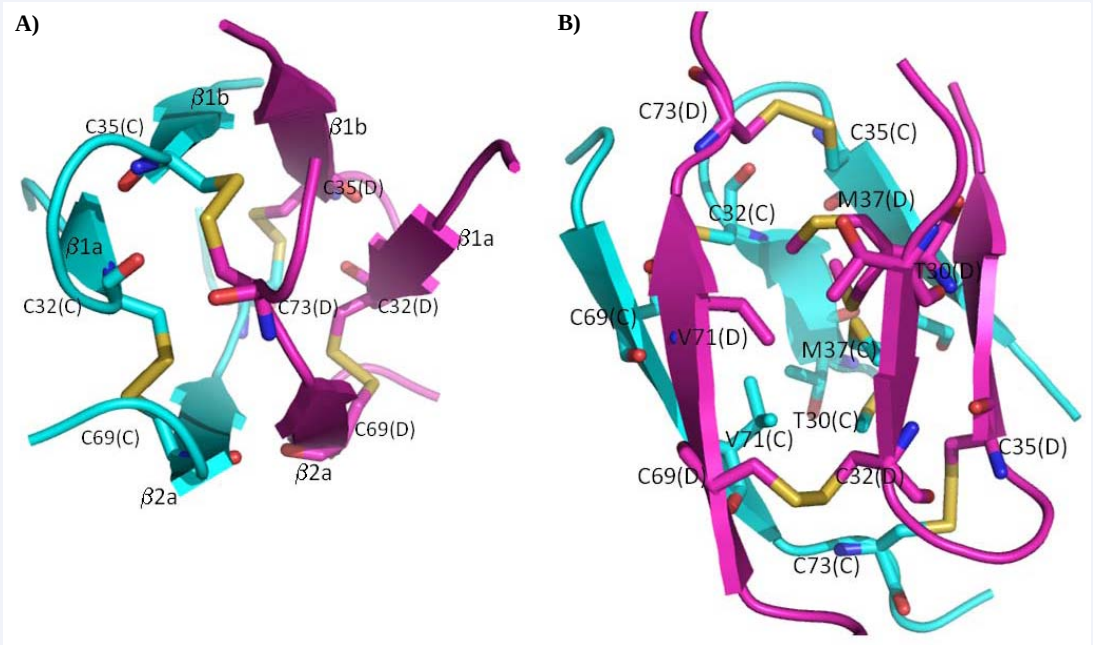

Figure 6 Ribbon diagram depicting the beta barrel motif observed at the interface of molecules C (pink) and D (cyan). (A) View down the center of the barrel showing the location of the four disulfide bridges that stabilize the barrel. Secondary structure elements are labeled. (B) View of the side of the barrel showing the location of the disulfide bridges and the residues occupying the core of the barrel.

An overlay of all six r-Trx-mesna structures (i.e., molecules A and B for the three structures determined) at Cys69 is shown in Figure 7A. The mesna-Cys69 adduct is occupying a large shallow pocket below α3' and above α0 along the face of the central β-sheet (Figure 7A). The mesna sulfonate is generally solvent exposed, and the six structures show multiple mesna binding orientations within this large pocket. Side chains near the ensemble of mesna orientations are Phe11, Gln12 and Glu70 (Figure 7A). Phe11 is generally rotated relative to its orientation in other published Trx structures, so as to accommodate the mesna-Cys69 adduct. Gln12 is bound in two general orientations. As depicted in Figure 7A (blue surface), Gln12 is pointing to the left in the pH 9.0/8.5 molecule B, pH 9.0/7.0 molecule B, pH 7.0/7.0 molecule B and pH 9.0/7.0 molecule A structures and is not involved in any hydrogen bonding interactions with the mesna. Gln12 is pointing to the right in the pH 9.0/8.5 molecule B and 7.0/7.0 molecule A structures and is within hydrogen bonding distance of the mesna sulfonate oxygen (3.3 Å) for the 9.0/8.5 structure (Figure 7A, orange surface). The distance between Gln12 NE2 and the sulfonate oxygen of mesna for the pH 7.0/7.0 structure is 4.4 Å. The carboxylate of Glu70 is pointing into the mesna binding pocket in some of the structures. However, Glu70 is rotated out of the pocket for the mesna orientations that would bring the sulfonate and carboxylate in close proximity.

The r-Trx pH 9.0/7.0 structure contains a second BNP7787-derived mesna adduct on Cys62 of molecules A and B. Cys62 is located at the end of α3 and is less solvent accessible than Cys69 (Figure 7B). There is a small shallow channel leading from solvent to Cys62 that is formed by the N-terminal ends of α3 and α0 which could partially stabilize the sulfonate of the mesna. There are no direct hydrogen bonds between the mesna sulfonate and the protein although given the low resolution of the structure, water mediated hydrogen bonds cannot be ruled out.

DISCUSSION

The goal of this work was to further evaluate the effect of BNP7787 on Trx activity and to identify the site(s) of adduct formation on Trx. In separate randomized multicenter Phase 2 and Phase 3 clinical trials in NSCLC, treatment with BNP7787 in combination with standard chemotherapy, resulted in substantial increases in the overall survival of patients with advanced adenocarcinoma sub-type NSCLC in the first line treatment setting [26]. Data indicate that Trx is a direct participant in the metabolism of BNP7787 and BN7787-derived mesna-disulfide heteroconjugates (Table 1). Enzyme assay data indicate that BNP7787 and BNP7787-derived mesna-disulfide heteroconjugates serve as alternative substrates that can act as inhibitors as they compete with endogenous substrates for Trx-mediated reduction (Table 1). We propose that BNP7787 and BNP7787-derived mesna-disulfide heteroconjugates may modulate the intracellular balance of oxidized (inactive) and reduced (active) Trx in vivo (Figure 8), and that BNP7787/Trx interactions may result in an increase in the inactive (oxidized) forms of Trx affecting the function of the natural Trx substrates that include reductases, transcription factors, and redox-dependent proteins (Figure 8) [6,9-11,36,37,43,44].

Sites of adduct formation were studied by mass spectroscopy and X-ray crystallography. MS studies identified possible BNP7787-derived mesna-cysteine mixed disulfides on Trx at Cys62, Cys69 and Cys73 (Figure 2). To unequivocally confirm the presence of adducts, crystallization experiments were pursued. To obtain crystals under conditions where the BNP7787-derived mesna-cysteine adducts were stable, we re-engineered Trx to raise the overall pI (wild-type protein yielded crystals exclusively at low, non-physiological pH where adducts were not stable). We completed the co-crystal structures under three different conditions which varied the pH of adduct formation and crystallization. All three structures showed an unusual tetrameric structure where two of the r-Trx molecules had the standard Trx fold and two had a previously unreported fold. The tetramer was tightly associated through a series of disulfide bridges and two of the molecules stabilized by a new beta barrel motif at the dimer

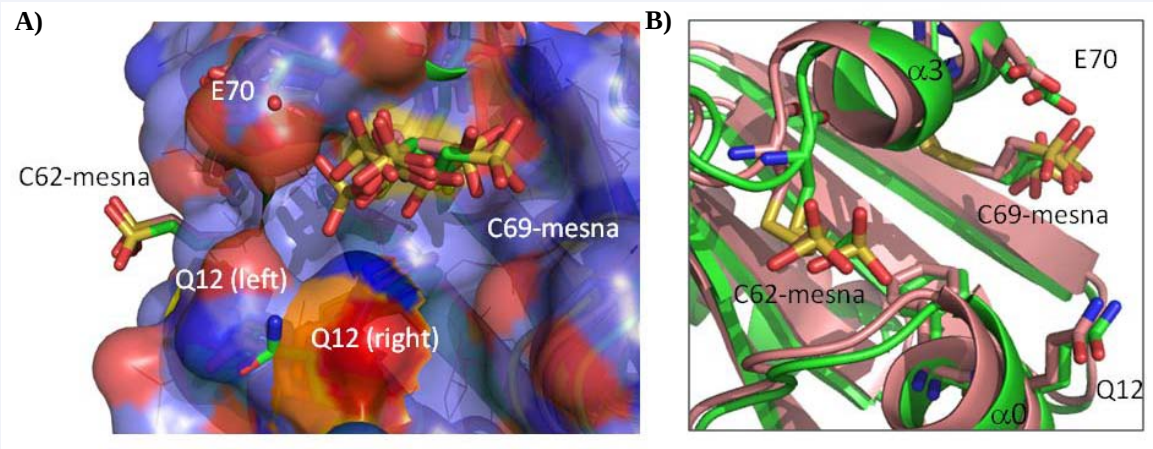

Figure 7 BNP7787-derived mesna adducts of r-Trx observed in these studies for molecules. (A) Overlay of all six r-Trx molecules which were modified by BNP7787 (molecules A and B for the three structures determined). Location of both mesna binding sites are shown with a focus on Cys69. The representative surface shown is for the r-Trx pH 9.0/8.5 molecule B structure. The orange surface is for Gln12 in the r-Trx pH 9.0/8.5 molecule A structure depicting the second major conformation observed for this residue (see text for detailed description). (B) Close-up of the Cys62 BNP7787-derived mesna adduct which was observed in the r-Trx pH 9.0/7.0 structure. Molecule B is shown in green and molecule A in pink. α3' and α0 are labeled and directed towards the mesna sulfonate.

interface (Figure 5D). BNP7787-derived mesna-cysteine adducts were found on Cys62 and Cys69 of molecules A and B which supported the results found in the MS studies. Cys73 was not available for adduct formation in the crystals as it was involved in a disulfide bridge at the tetramer interface. Hence, the MS and x-ray data are in general agreement and the first x-ray structure data clearly demonstrating a stable, small molecule-derived mixed disulfide on human Trx is reported herein.

The Trx structures described herein are, to our knowledge, the first reported crystal structures showing a small molecule-derived, mixed disulfide covalently-associated with human Trx. The structure of Trx containing peptide-derived mixed disulfides has been solved [45,46], and a co-crystal of plant Trx in complex with the BASI protein has been reported [47]. More recently, the structure of Trx in complex with TrxR has been reported (**PDB ID: 3QFA and 3QFB**) [48]. Additionally, Weischel et al., crystallized human Trx containing nitrosylated Cys62 and Cys69 residues [49,50]. For the reported Trx structures to date varying degrees of conformational shifts have been observed; however, in these structures the overall "core" Trx fold remains quite similar. The tetrameric Trx structure we report herein appears to be structurally quite novel as discussed below.

The oligomeric state of Trx in solution was studied by native gels. Native gel analyses of Trx incubated with BNP7787 showed distinct protein bands consistent with a tetramer and a dimer. The presence of a tetramer is in agreement with the x-ray structure, and the mixture of tetramer and dimer could explain the minor distinctions between the MS and x-ray data. Trx incubated with buffer only was smeared, migrated larger than a tetramer, and the extent of smearing increased with the incubation time (Figure 3B). Based on our observations, in solution with the absence of a reductant such as dithiothreitol or β-mercaptoethanol, various oligomeric forms of Trx can form and are difficult to characterize using gel-based or solution-based analytic approaches. However, other tetrameric forms of Trx have been observed by X-ray crystallography [49], and X-ray crystallography may represent the best approach to capture unusual Trx oligomers like the tetramer reported herein.

In addition to the BNP7787-derived mesna adducts, we observe the formation of a number of new inter- and intra-molecular disulfide bridges. Many of these are involved in stabilizing the tetramer. Unusual disulfide bonding has been reported by Hall and Emsley for Trx proteins that have mutated cysteine residues (C35S, C73R, see **PDB ID: 3E3E**) resulting in two intermolecular disulfide bonds between the two molecules in the dimer: a) Cys32 - Cys69, and b) Cys32 - Cys62. For both molecules, the α3 helix containing Cys62 and Cys69 unraveled although the conformational change was much less dramatic than what we report herein [51]. In another study by Weichsel et al, two mutations were introduced (C69S, C73S). In the reduced form, the Trx fold was maintained however for oxidized protein, a tetramer was formed which consisted of the more commonly observed Trx dimer and a new dimer interface formed by an

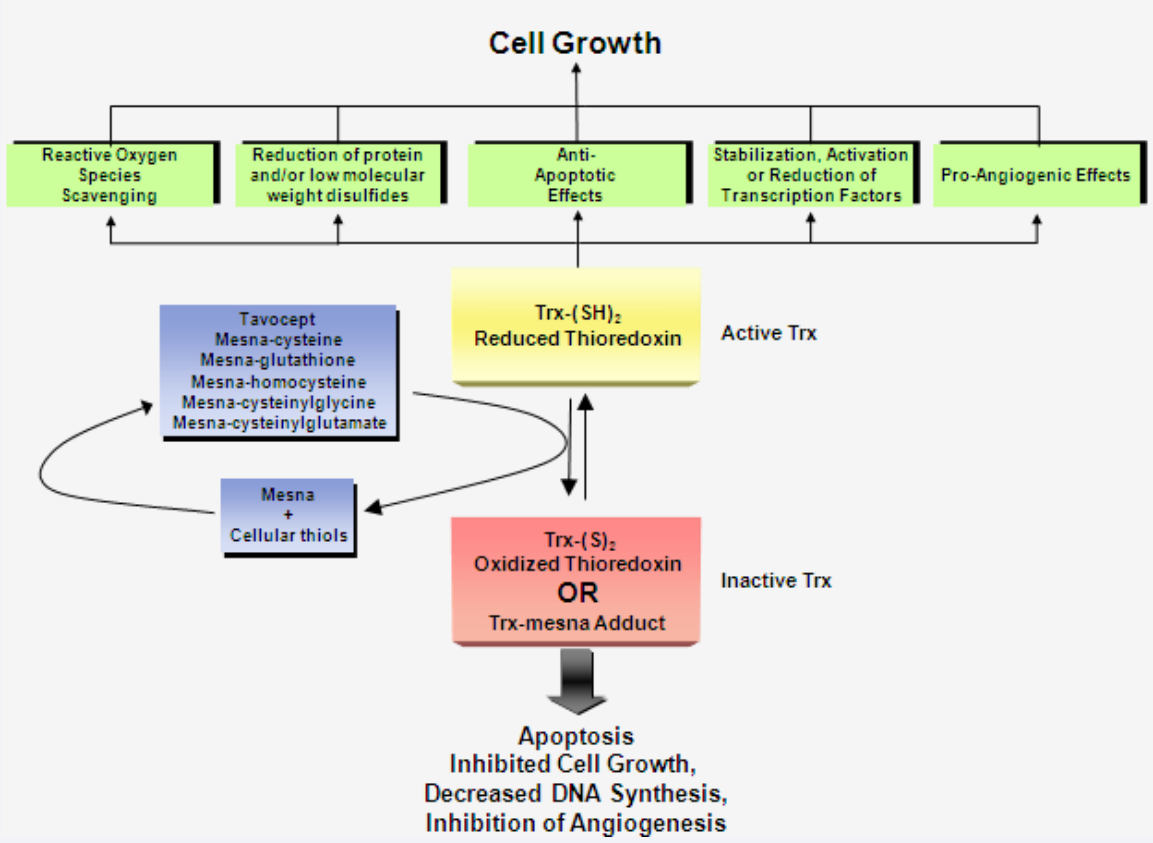

Figure 8 Model of how BNP7787 (Tavocept®) and BNP7787-derived heteroconjugates may help modulate the intracellular balance of oxidized (inactive) and reduced (active) Trx. (See Figure 1 for chemical structures of BNP7787 and the BNP7787 heteroconjugates.)

Table 2: Image processing statistics (HKL 2000 or Mosflm).

	r-Trx pH 9.0/8.5	r-Trx pH 9.0/7.0	r-Trx pH 7.0/7.0
Unit cell length (a,b,c Å)	125.5 92.0 57.6	85.5 57.9 94.9	44.5 91.8 57.1
Unit cell angles (α, β, γ°)	90 108.4 90	90 90.3 90	90 105 90
Space group	C2	C2	$P2_1$
Resolution (Å)	48.6 – 2.50 (2.64-2.50)[1]	47.9 – 2.80 (2.95 -2.80)[1]	50.0 – 2.5 (1.92 -1.85)[1]
Total no. data	93111	32088	141829
No. unique data	21540	11124	37414
Completeness	99.9 (99.9)[1]	96.1 (92.1)[1]	100.0 (100.0)[1]
Multiplicity	4.3 (4.4)[1]	2.9 (2.4)[1]	3.8 (3.8)[1]
Rmerge	0.090 (0.622)[1]	0.095 (0.396)[1]	0.064 (0.595)[1]
Mean I/σ(I)	8.7 (2.1)[1]	8.5 (2.2)[1]	19.4 (2.3)[1]

[1]Data in parenthesis are for the outer resolution shell.

Table 3: Refinement statistics for final structures.

	r-Trx pH 9.0/8.5	r-Trx pH 9.0/7.0	r-Trx pH 7.0/7.0
Resolution (Å)	48.4 – 2.50	47.950 – 2.80	36.114 – 1.855
No. data used	21535	10588	35518
No. atoms	3307	3313	3520
No. residues	424	424	428
No. protein chains	4	4	4
R value	0.24	0.2446	0.213
Rfree value	0.29	0.3128	0.2615
Mean B-value (Å²)	46.5	27.592	28.14
RMSD bonds (Å)	0.011	0.006	0.014
RMSD angles (°)	1.272	0.882	1.370
No. Phi-psi outliers	8	6	3

intermolecular disulfide bond between Cys62 residues of the two Trx molecules (**PDB ID: 3M9K**). In one Trx molecule, the Cys62 is part of an intact α3 helix whereas in the other Trx molecule the α3 helix is partially unraveled [49]. The tetramer in this structure is a dimer of dimers and is different from the tetramer reported herein. In our studies, no Trx cysteine residues were mutated, and we attribute the scrambled disulfide pattern and Trx tetramer we observed to BNP7787-related modification of Trx consistent with the results obtained in our native gel studies. Nonetheless, there is precedent for structural shifts of the standard Trx fold. These conformational changes include α3 which is also affected in our structures. However, unlike previous studies, we do not attribute the structural changes observed for our structure to the mutations we introduced to facilitate high pH crystallization. The mutations in our reported TRX structures are remote from both the conformational shifts we observed and the newly formed tetramer interface. Furthermore, the mutations do not involve cysteine residues, and our LC-MS and activity characterization studies show similar results for both WT Trx and r-Trx.

CONCLUSION

We propose that the in vitro interactions described herein between Trx and BNP7787 may be important in terms of their effect on Trx functioning in vivo. Trx interacts with a wide range of cellular macromolecules and modulation of Trx is important for regulating cell growth, apoptosis, RNA to DNA conversion, transcription factor signaling and protection from oxidative stress (Figure 8 and discussion herein). Formation of a BNP7787-derived cysteine-mesna adduct on Trx could modulate one or more of these interactions affecting cellular signaling and contributing to the effects observed in the clinic.

We have characterized related BNP7787-mediated effects and cysteine modification on multiple other protein targets, and in each case, the effect is correlated with the role of the modified cysteine residues in protein structure and/or function (manuscripts in preparation). We propose that BNP7787-mediated mixed-disulfide formation on select proteinaceous cysteine residues, resulting in altered molecular properties and/or function, may be a general mechanism of action for BNP7787. This process represents a novel mechanism of action for this type of agent; however, cysteine-specific, post-translational modifications of cysteine residues in proteins, are a biological mechanism that may regulate a variety of cellular processes and includes glutathionylation, nitrosylation, prenylation, and palmitoylation [32]. Some of these cysteine-modification processes are autocatalytic, like BNP7787-mediated modification of cysteine residues, cysteine nitrosylation, and

many cases of glutathionylation, while others require protein cofactors (e.g. prenylation). Clearly cysteines within proteins have varied functional and structural roles, and molecules that modulate cysteine function have the potential to be useful as chemosupportive and/or anticancer agents.

ACKNOWLEDGEMENTS

We thank Banumathi Sankaran, and Peter Zwart (Berkeley Center for Structural Biology, Lawrence Berkeley National Laboratory) for assistance with data collection. The Berkeley Center for Structural Biology is supported in part by the National Institutes of Health, National Institute of General Medical Sciences, and the Howard Hughes Medical Institute. The Advanced Light Source is supported by the Director, Office of Science, Office of Basic Energy Sciences, of the U.S. Department of Energy under Contract No. DE-AC02-05CH11231. We thank Rick Walter and Gina Ranieri (Shamrock Structures) for data collection at the Advanced Photon Source, and Xinghai Chen and Qiuli Huang (BioNumerik Pharmaceuticals, Inc.) for synthesis of BNP7787 and BNP7787-related disulfides. We gratefully acknowledge the LC-MS analyses of tryptic fragments by the late Dr. Su Chen (BioNumerik Pharmaceuticals, Inc.).

Conflict of Interest

Employment or leadership position: Aulma Parker, Pavan Petluru, Betsy Leverett, Philippe Ayala, Min Zhao, Kamwing Jair, Harry Kochat, Frederick Hausheer; BioNumerik Pharmaceuticals, Inc. Vicki Nienaber, Vandana Sridhar, Barbara Chie-Leon, John Badger; Zenobia Therapeutics, Inc.

REFERENCES

1. Pedone E, Limauro D, D'Ambrosio K, De Simone G, Bartolucci S. Multiple catalytically active thioredoxin folds: a winning strategy for many functions. Cell Mol Life Sci. 2010; 67: 3797-3814.
2. Atkinson HJ, Babbitt PC. An atlas of the thioredoxin fold class reveals the complexity of function-enabling adaptations. PLoS Comput Biol. 2009; 5: e1000541.
3. Forman-Kay JD, Clore GM, Wingfield PT, Gronenborn AM. High-resolution three-dimensional structure of reduced recombinant human thioredoxin in solution. Biochemistry. 1991; 30: 2685-2698.
4. Weichsel A, Gasdaska JR, Powis G, Montfort WR. Crystal structures of reduced, oxidized, and mutated human thioredoxins: evidence for a regulatory homodimer. Structure. 1996; 4: 735-751.
5. Tamura T, Stadtman TC. A new selenoprotein from human lung adenocarcinoma cells: purification, properties, and thioredoxin reductase activity. Proc Natl Acad Sci U S A. 1996; 93: 1006-1011.
6. Holmgren A. Thioredoxin and glutaredoxin systems. J Biol Chem. 1989; 264: 13963-13966.
7. Biaglow JE, Miller RA. The thioredoxin reductase/thioredoxin system: novel redox targets for cancer therapy. Cancer Biol Ther. 2005; 4: 6-13.
8. Becker K, Gromer S, Schirmer RH, Müller S. Thioredoxin reductase as a pathophysiological factor and drug target. Eur J Biochem. 2000; 267: 6118-6125.
9. Powis G, Mustacich D, Coon A. The role of the redox protein thioredoxin in cell growth and cancer. Free Radic Biol Med. 2000; 29: 312-322.
10. Prieto-Alamo MJ, Jurado J, Gallardo-Madueno R, Monje-Casas F, Holmgren A, Pueyo C. Transcriptional regulation of glutaredoxin and thioredoxin pathways and related enzymes in response to oxidative stress. J Biol Chem. 2000; 275: 13398-13405.
11. Jacob C, Giles GI, Giles NM, Sies H. Sulfur and selenium: the role of oxidation state in protein structure and function. Angew Chem Int Ed Engl. 2003; 42: 4742-4758.
12. Arnér ES, Holmgren A. Physiological functions of thioredoxin and thioredoxin reductase. Eur J Biochem. 2000; 267: 6102-6109.
13. Powis G, Kirkpatrick DL. Thioredoxin signaling as a target for cancer therapy. Curr Opin Pharmacol. 2007; 7: 392-397.
14. Holmgren A, Lu J. Thioredoxin and thioredoxin reductase: current research with special reference to human disease. Biochem Biophys Res Commun. 2010; 396: 120-124.
15. Boven E, Verschraagen M, Hulscher TM, Erkelens CA, Hausheer FH, Pinedo HM, et al. BNP7787, a novel protector against platinum-related toxicities, does not affect the efficacy of cisplatin or carboplatin in human tumour xenografts. Eur J Cancer. 2002; 38: 1148-1156.
16. Boven E, Westerman M, van Groeningen CJ, Verschraagen M, Ruijter R, Zegers I, et al. Phase I and pharmacokinetic study of the novel chemoprotector BNP7787 in combination with cisplatin and attempt to eliminate the hydration schedule. Br J Cancer. 2005; 92: 1636-1643.
17. Hausheer FH, Kanter P, Cao S, Haridas K, Seetharamulu P, Reddy D, et al. Modulation of platinum-induced toxicities and therapeutic index: mechanistic insights and first- and second-generation protecting agents. Semin Oncol. 1998; 25: 584-599.
18. Hausheer FH, Kochat H, Parker AR, Ding D, Yao S, Hamilton SE, et al. New approaches to drug discovery and development: a mechanism-based approach to pharmaceutical research and its application to BNP7787, a novel chemoprotective agent. Cancer Chemother Pharmacol. 2003; 52 Suppl 1: S3-15.
19. Pendyala L, Schwartz G, Smith P, Zdanowicz J, Murphy M, Hausheer F. Modulation of plasma thiols and mixed disulfides by BNP7787 in patients receiving paclitaxel/cisplatin therapy. Cancer Chemother Pharmacol. 2003; 51: 376-384.
20. Verschraagen M, Boven E, Ruijter R, van der Born K, Berkhof J, Hausheer FH, et al. Pharmacokinetics and preliminary clinical data of the novel chemoprotectant BNP7787 and cisplatin and their metabolites. Clin Pharmacol Ther. 2003; 74: 157-169.
21. Verschraagen M, Boven E, Torun E, Erkelens CA, Hausheer FH, van der Vijgh WJ. Pharmacokinetic behaviour of the chemoprotectants BNP7787 and mesna after an i.v. bolus injection in rats. Br J Cancer. 2004; 90: 1654-1659.
22. Verschraagen M, Boven E, Torun E, Hausheer FH, Bast A, van der Vijgh WJ. Possible (enzymatic) routes and biological sites for metabolic reduction of BNP7787, a new protector against cisplatin-induced side-effects. Biochem Pharmacol. 2004; 68: 493-502.
23. Verschraagen M, Boven E, Zegers I, Hausheer FH, Van der Vijgh WJ. Pharmacokinetics of BNP7787 and its metabolite mesna in plasma and ascites: a case report. Cancer Chemother Pharmacol. 2003; 51: 525-529.
24. Verschraagen M, Kedde MA, Hausheer FH, Van Der Vijgh WJ. The chemical reactivity of BNP7787 and its metabolite mesna with the cytostatic agent cisplatin: comparison with the nucleophiles thiosulfate, DDTC, glutathione and its disulfide GSSG. Cancer Chemother Pharmacol. 2003; 51: 499-504.
25. Verschraagen M, Zwiers TH, de Koning PE, Welink J, van der Vijgh WJ. Quantification of BNP7787 (dimesna) and its metabolite mesna in human plasma and urine by high-performance liquid chromatography with electrochemical detection. J Chromatogr B Biomed Sci Appl. 2001; 753: 293-302.

26. Hausheer F, Bain S, Perry M, Du L, Ohashi Y, Ariyoshi Y, Fukuoka M. Comprehensive Meta-Analysis of Survival Outcomes from Two Randomized Multicenter Trials in First-Line Advanced Non-Small Cell Lung Cancer in Patients Treated with the Novel Investigational Antitumor-enhancing and Chemoprotective Agent Tavocept. Eur J.Clin.Med.Oncol, 2009, 2:7-19.

27. Hausheer FH, Ding D, Shanmugarajah D, Leverett BD, Huang Q, Chen X, et al. Accumulation of BNP7787 in human renal proximal tubule cells. J Pharm Sci. 2011; 100: 3977-3984.

28. Shanmugarajah D, Ding D, Huang Q, Chen X, Kochat H, Petluru PN, et al. Analysis of BNP7787 thiol-disulfide exchange reactions in phosphate buffer and human plasma using microscale electrochemical high performance liquid chromatography. J Chromatogr B Analyt Technol Biomed Life Sci. 2009; 877: 857-866.

29. Go YM, Jones DP. The redox proteome. J Biol Chem. 2013; 288: 26512-26520.

30. Grek CL, Zhang J, Manevich Y, Townsend DM, Tew KD. Causes and consequences of cysteine S-glutathionylation. J Biol Chem. 2013; 288: 26497-26504.

31. Chung HS, Wang SB, Venkatraman V, Murray CI, Van Eyk JE. Cysteine oxidative posttranslational modifications: emerging regulation in the cardiovascular system. Circ Res. 2013; 112: 382-392.

32. Pace NJ, Weerapana E. Diverse functional roles of reactive cysteines. ACS Chem Biol. 2013; 8: 283-296.

33. Rajca A and Wiessler M. Synthesis of asymmetric disulfides with thiol sulfonates immobilized on a polystyrene support. Tetrahedron Lett. 1999; 31: 6075-6077.

34. Holmgren A. Reduction of disulfides by thioredoxin. Exceptional reactivity of insulin and suggested functions of thioredoxin in mechanism of hormone action. J Biol Chem. 1979; 254: 9113-9119.

35. Murshudov GN, Vagin AA, Dodson EJ. Refinement of macromolecular structures by the maximum-likelihood method. Acta Crystallogr D Biol Crystallogr. 1997; 53: 240-255.

36. Holmgren A. Thioredoxin catalyzes the reduction of insulin disulfides by dithiothreitol and dihydrolipoamide. J Biol Chem. 1979; 254: 9627-9632.

37. Luthman M, Holmgren A. Rat liver thioredoxin and thioredoxin reductase: purification and characterization. Biochemistry. 1982; 21: 6628-6633.

38. Mustacich D, Powis G. Thioredoxin reductase. Biochem J. 2000; 346 Pt 1: 1-8.

39. Casagrande S, Bonetto V, Fratelli M, Gianazza E, Eberini I, Massignan T, et al. Glutathionylation of human thioredoxin: a possible crosstalk between the glutathione and thioredoxin systems. Proc Natl Acad Sci U S A. 2002; 99: 9745-9749.

40. Han S. Force field parameters for S-nitrosocysteine and molecular dynamics simulations of S-nitrosated thioredoxin. Biochem Biophys Res Commun. 2008; 377: 612-616.

41. Kirkpatrick DL, Kuperus M, Dowdeswell M, Potier N, Donald LJ, Kunkel M, et al. Mechanisms of inhibition of the thioredoxin growth factor system by antitumor 2-imidazolyl disulfides. Biochem Pharmacol. 1998; 55: 987-994.

42. Pan JL, Bardwell JC. The origami of thioredoxin-like folds. Protein Sci. 2006; 15: 2217-2227.

43. Powis G, Briehl M, Oblong J. Redox signalling and the control of cell growth and death. Pharmacol Ther. 1995; 68: 149-173.

44. Powis G, Montfort WR. Properties and biological activities of thioredoxins. Annu Rev Biophys Biomol Struct. 2001; 30: 421-455.

45. Qin J, Clore GM, Kennedy WM, Huth JR, Gronenborn AM. Solution structure of human thioredoxin in a mixed disulfide intermediate complex with its target peptide from the transcription factor NF kappa B. Structure, 1995, 3:289-297.

46. Qin J, Clore GM, Kennedy WP, Kuszewski J, Gronenborn AM. The solution structure of human thioredoxin complexed with its target from Ref-1 reveals peptide chain reversal. Structure. 1996; 4: 613-620.

47. Maeda K, Hägglund P, Finnie C, Svensson B, Henriksen A. Structural basis for target protein recognition by the protein disulfide reductase thioredoxin. Structure. 2006; 14: 1701-1710.

48. Fritz-Wolf K, Kehr S, Stumpf M, Rahlfs S, Becker K. Crystal structure of the human thioredoxin reductase-thioredoxin complex. Nat Commun. 2011; 2: 383.

49. Weichsel A, Kem M, Montfort WR. Crystal structure of human thioredoxin revealing an unraveled helix and exposed S-nitrosation site. Protein Sci. 2010; 19: 1801-1806.

50. Weichsel A, Brailey JL, Montfort WR. Buried S-nitrosocysteine revealed in crystal structures of human thioredoxin. Biochemistry. 2007; 46: 1219-1227.

51. Hall G, Emsley J. Structure of human thioredoxin exhibits a large conformational change. Protein Sci. 2010; 19: 1807-1811.

Cite this article

Parker AR, Nienaber VL, Petluru PN, Sridhar V, Leverett BD, et al. (2014) BNP7787 Forms Novel Covalent Adducts on Human Thioredoxin and Modulates Thioredoxin Activity. J Pharmacol Clin Toxicol 2(2):1026.